

CycleVLA: Proactive Self-Correcting Vision-Language-Action Models via Subtask Backtracking and Minimum Bayes Risk Decoding

Chenyang Ma¹, Guangyu Yang², Kai Lu¹, Shitong Xu¹,
Bill Byrne², Niki Trigoni¹, Andrew Markham¹

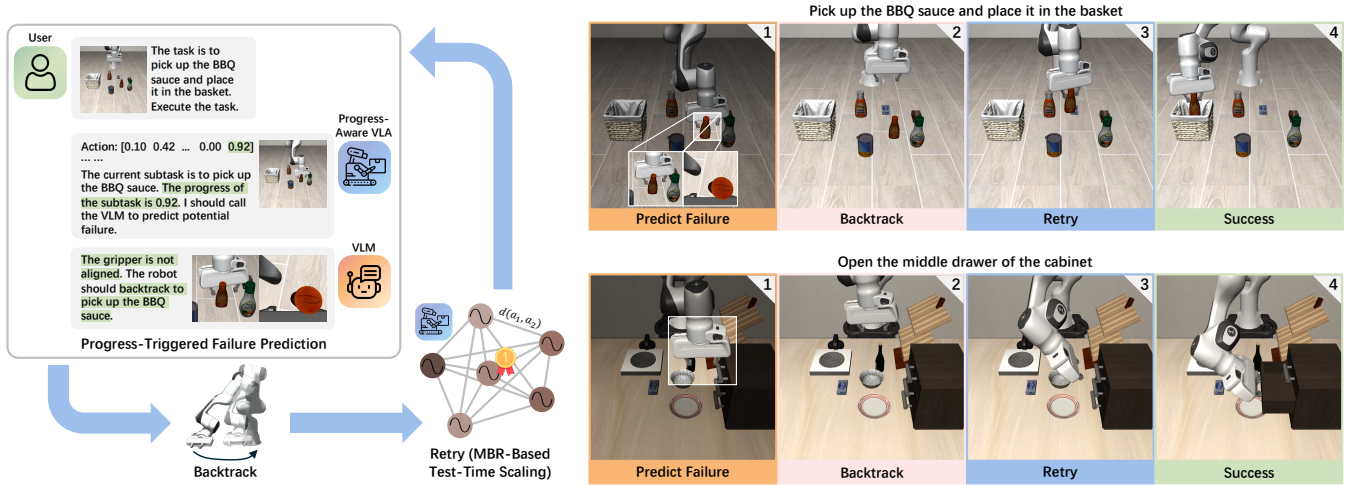


Fig. 1: **Vision-Language-Action models with proactive self-correction capabilities.** We introduce **CycleVLA**, which enables VLAs to anticipate incipient failures and recover before execution collapses. CycleVLA first augments a VLA to estimate subtask-level progress and flag critical subtask transition points, where failures most frequently occur. Then, at these points during inference, a VLM is queried to predict whether the current execution will fail and to decide whether to backtrack. Upon backtracking, the VLA retries using test-time scaling via Minimum Bayes Risk decoding to improve success. This cycle repeats until the task succeeds or execution terminates.

Abstract—Current work on robot failure detection and correction typically operate in a post hoc manner, analyzing errors and applying corrections only after failures occur. This work introduces CycleVLA, a system that equips Vision-Language-Action models (VLAs) with proactive self-correction, the capability to anticipate incipient failures and recover before they fully manifest during execution. CycleVLA achieves this by integrating a progress-aware VLA that flags critical subtask transition points where failures most frequently occur, a VLM-based failure predictor and planner that triggers subtask backtracking upon predicted failure, and a test-time scaling strategy based on Minimum Bayes Risk (MBR) decoding to improve retry success after backtracking. Extensive experiments show that CycleVLA improves performance for both well-trained and under-trained VLAs, and that MBR serves as an effective zero-shot test-time scaling strategy for VLAs.

I. INTRODUCTION

Humans constantly adjust their actions when they sense something going wrong, such as tightening their grip when a glass begins to slip, or adjusting the steering wheel before drifting out of a lane. These corrections happen during the act, not after, because a shattered glass cannot be recovered, and a car off the road is already in danger. Once an error has fully occurred, the opportunity for correction has passed.

We call this *proactive self-correction* [1], the ability to detect incipient errors during execution and adapt before failure fully manifests. Replicating this ability in robot agents remains an open challenge. For instance, such a robot should recognize that a grasp is misaligned and reposition its gripper before knocking the object over, completing the task within the execution episode without external intervention. This stands in contrast to most recent work on robot failure detection and correction, which operates in a post hoc manner: execution failures are identified only as or after they occur [2]–[8], and corrective actions are applied retrospectively, often as residual policies [9]–[12].

In this work, we aim to equip generalist robot foundation models, specifically Vision-Language-Action models (VLAs) [13]–[15], with proactive self-correcting capabilities, as shown in Fig. 1. Our approach, **CycleVLA**, is motivated by the observation that many robot task failures occur at subtask transitions [16]–[20], and that progress near subtask completion provides strong cues for anticipating such failures (e.g., one can tell a peg is misaligned before it jams during insertion). Based on this insight, CycleVLA first introduces a finetuning pipeline that endows VLAs with explicit awareness of subtask progress, addressing a key limitation of existing VLAs that lack mechanisms for stopping or progress estimation [19]. We achieve this by decomposing

¹Department of Computer Science, University of Oxford

²Department of Engineering, University of Cambridge

demonstrations into aligned subtasks and finetuning the VLA with extended action dimensions that predict both a stop signal and subtask progress.

With a progress-aware VLA, the next challenge is deciding whether to transition to the next subtask or intervene near subtask termination, before failure occurs. CycleVLA addresses this through an explicit backtracking mechanism [21]–[23] guided by a Vision-Language Model (VLM) [24]–[28]. At test time, the VLM acts as a zero-shot failure predictor and planner: if no failure is predicted, execution continues; otherwise, the system reverts to the earliest subtask that restores missing preconditions and retries.

Finally, to improve the success of retries after backtracking, CycleVLA adopts a zero-shot test-time scaling strategy based on Minimum Bayes Risk (MBR) decoding [29]. Since most VLAs are trained via imitation learning [13], [30], [31], successful behaviors tend to cluster in high-density regions of the policy output space [32], [33], which makes consensus selection over multiple samples more likely to succeed. Inspired by recent applications of MBR decoding in large language models (LLMs) at inference time [34]–[36], we sample multiple trajectories from the VLA and select the one that minimizes expected risk under a distance metric.

In summary, our main contributions are threefold:

- We introduce CycleVLA, a system that enables proactive self-correction in VLAs by combining (a) a finetuning pipeline that extends VLAs with subtask progress prediction, (b) a VLM-based failure predictor and planner that uses progress cues to decide if to transit or backtrack between subtasks, and (c) a MBR-based test-time scaling strategy that improves recovery after backtracking.
- We demonstrate that MBR decoding serves as a zero-shot test-time scaling strategy for improving the success rate of VLA policies.
- Extensive experiments show that CycleVLA effectively improves task success across robot benchmarks and remains effective when applied to under-trained VLAs.

II. RELATED WORK

A. Robot Failure Detection and Correction

Most prior work addresses robot failure detection in isolation. Given the scarcity of robot failure data, many approaches rely on failures observed at inference time, using conformal prediction [2], [5], [8], [37], [38], state-based anomaly detection [1], [4], [39], [40], or LLMs/VLMs for failure recognition [3], [5], [41]–[43]. Another line of work studies post hoc failure correction, applying retrospective analysis and residual recovery policies after failures occur [9]–[12], [44]. More recent work explores proactive correction during execution, such as combining visuomotor policies with visual world models to anticipate future states [45]–[48], but these incur substantial overhead and architectural changes. In contrast, our work equips generalist robot foundation models with proactive self-correction via explicit VLM-based failure prediction, subtask-level backtracking [21]–[23], and retry. The closest works are PAINT [1] and Bellman-Guided

Retrials [23], but PAINT requires human intervention and the latter does not target generalist policies.

B. Data Augmentation for VLAs

VLA training lacks a standard data augmentation strategy, and recent work explores several directions. To tackle long-horizon tasks, some approaches decompose demonstrations into subtasks [16]–[20], [49], [50], with the active subtask inferred at inference by an external system [18] or the VLA itself [17], [51]. Some works incorporate textual reasoning into training to enable explicit reasoning at inference [51]–[54]. Visual augmentation has also been explored: Cosmos [55] applies video style transfer, while others highlight task-relevant objects [56], [57], akin to visual prompting in VLMs [58]. Our work also adopts subtask decomposition, but specifically focuses on teaching VLAs when to stop at subtask transitions and to track their own progress—capabilities largely absent from existing VLAs [19].

C. Test-Time Scaling for VLAs

Test-time scaling has proven effective for LLMs [59]–[61], and recent work explores its application to VLAs. RoboMonkey [32] samples actions with Gaussian perturbations and uses a trained VLM to select among candidates. Rover [33] and V-GPS [62] score sampled actions using learned reward or value models. In contrast, our MBR decoding [29], inspired by its use in LLMs [34]–[36], performs training-free consensus selection without external verifiers.

III. PRELIMINARIES

We consider sequential decision-making with the current observation o_t (e.g., RGB images and proprioception) and a natural language goal g . A VLA policy π_θ maps (o_t, g) to robot actions. We adopt a continuous end-effector delta action representation $a_t = [\Delta x_t, \Delta y_t, \Delta z_t, \Delta u_t, \Delta v_t, \Delta w_t, \gamma_t]^\top \in \mathbb{R}^7$, where $(\Delta x_t, \Delta y_t, \Delta z_t) \in \mathbb{R}^3$ and $(\Delta u_t, \Delta v_t, \Delta w_t) \in \mathbb{R}^3$ denote translational and rotational displacements, and $\gamma_t \in \{0, 1\}$ indicates the gripper state. Unlike autoregressive formulations, we assume the VLA employs parallel decoding to produce a continuous chunk of future actions in a single forward pass, i.e., $\pi_\theta(a_{t:t+H-1} \mid o_t, g)$ for chunk size H . At inference time, we further assume the policy supports stochastic decoding, enabling the generation of a finite set of action sequence hypotheses $\mathcal{A} = \{a_{t:t+H-1}^{(1)}, \dots, a_{t:t+H-1}^{(N)}\}$ via repeated forward passes (e.g., stochastic latent variables, diffusion-based noise sampling).

IV. CYCLEVLA

Our goal is to equip VLAs with proactive self-correction capabilities. Our approach, CycleVLA (Fig. 3), builds on the observation that task failures often occur at subtask transitions, where progress near completion provides strong cues for anticipating failure. We first introduce a finetuning pipeline that constructs a subtask-decomposed dataset from demonstrations and trains VLAs to explicitly predict stop and progress signals with lightweight modifications (Sec. IV-A). At inference time, we use an off-the-shelf VLM as a

failure predictor and planner to decide whether to transition or backtrack at subtask boundaries (Sec. IV-B). Finally, we apply MBR decoding as a zero-shot test-time scaling strategy to improve retry success after backtracking (Sec. IV-B).

A. Learning Stop and Progress Signals for Subtask Execution

Constructing a Subtask-Decomposed Dataset. We introduce a pipeline that uses LLMs to decompose demonstrations into subtasks with precise start/end timestamps and language instructions (Fig. 2), inspired by prior work [16], [51].

Given a task instruction g , we first prompt an LLM to decompose it into a minimal sequence of atomic subtasks (g_1, \dots, g_K) using a constrained action vocabulary (e.g., move, rotate, open, close). In parallel, we extract per-step gripper states (open, close, or idle) and movement primitives (e.g., move forward, rotate clockwise, stop) [51] from robot proprio by computing state differences over a sliding window.

We then align subtasks to the trajectory using gripper state transition segments, which provide reliable subtask boundaries in manipulation tasks (e.g., continuous open/close segments correspond to grasping or releasing objects, while idle segments typically indicate periods of robot translational or rotational motion with no gripper actuation). If the number of LLM-proposed subtasks matches the number of gripper state segments, we directly pair each subtask with the corresponding segment timestamps. Otherwise, we prompt an LLM with the extracted movement primitive sequence (downsampled to a fixed maximum length to reduce context length) to infer subtask timestamp boundaries, enforcing continuous assignment without gaps while filtering spurious stop or inconsistent primitives.

Subtask Finetuning with Extended Action Dims. With the subtask-decomposed dataset, we finetune the VLA with extended action dimensions to predict stop and progress signals—capabilities not explicitly modeled in existing VLAs [19]. We extend the 7-dim action a_t to 9-dim: $a_t = [\Delta x_t, \Delta y_t, \Delta z_t, \Delta u_t, \Delta v_t, \Delta w_t, \gamma_t, s_t, p_t]^\top \in \mathbb{R}^9$, where $s_t \in \{0, 1\}$ denotes a stop signal indicating subtask termination, and $p_t \in [0, 1]$ denotes subtask progress, discretized into bins of 0.1 based on the normalized timestep within each subtask. We explicitly separate these two signals because the stop signal must be precise to support correct subtask transitions, whereas the progress signal only needs to indicate proximity to subtask completion. Following NaVILA [63], we oversample the last action step of each subtask during training to emphasize termination detection. At inference time, we binarize s_t via thresholding, as with the gripper signal γ_t .

We predict stop and progress jointly with end-effector delta actions as scalar outputs, rather than introducing separate classification heads. This design aligns with the continuous nature of the VLA action space: end-effector displacements are floating-point values, and the gripper signal γ_t is a bounded scalar. Predicting s_t and p_t in the same output space therefore requires no architectural changes beyond widening the action dimension.

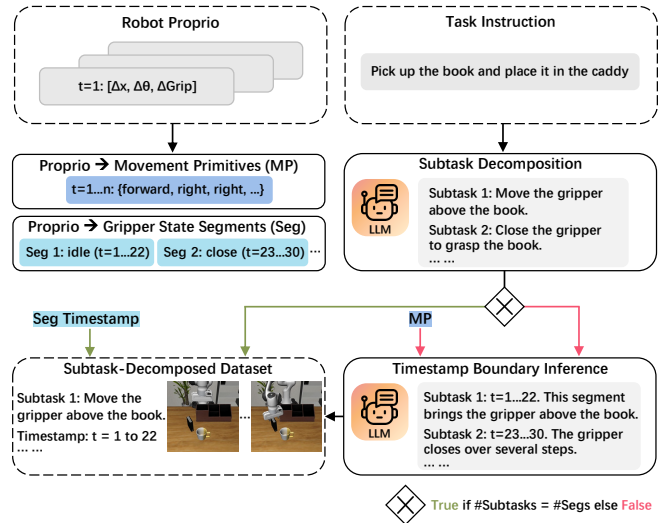


Fig. 2: **Pipeline for constructing the subtask-decomposed dataset.** Following LLM subtask decomposition and extraction of movement primitives and gripper state segments, subtasks are directly aligned to gripper state segment timestamps when their counts match; otherwise, an LLM infers subtask boundaries from the movement primitive sequence. Please see Appendices B and E for more details.

B. Test-Time Scaling via Subtask Backtrack and MBR Decode

VLM as a Failure Predictor and Planner. With a progress-aware VLA, we use an off-the-shelf VLM to predict failure and plan recovery at subtask boundaries. When the VLA-predicted progress reaches τ_p , we query the VLM with synchronized third-person and wrist-mounted camera views, the current subtask, and the subtask list. The VLM outputs one of two decisions: transit to the next subtask, or backtrack to the earliest subtask that restores missing preconditions (e.g., if the grasped object drops midway, backtrack to the grasping subtask). We include both views so the VLM can leverage global context from the third-person view (e.g., object identity, gripper pose, if the correct subtask is being executed) and fine-grained cues from the wrist view (e.g., gripper alignment with the object, contact quality), outputting Chain-of-Thought reasoning [64] that fuses evidence from both views.

When backtracking is triggered, we restore the robot state to the beginning of the target subtask by reverse-executing recorded delta actions [23].

Sampling Actions and Ranking via MBR. After backtracking restores a valid subtask precondition, the VLA retries the subtask from the same start state. We apply test-time scaling by sampling multiple action chunk hypotheses and selecting a consensus one via MBR decoding [29]. From current observation o_t and subtask g_k , we draw N hypotheses $\mathcal{A} = \{a_{t:t+H-1}^{(1)}, \dots, a_{t:t+H-1}^{(N)}\}$ from the stochastic policy $\pi_\theta(\cdot | o_t, g_k)$.

MBR selects the hypothesis that minimizes the expected risk under the policy distribution. Let $d(\cdot, \cdot)$ denote the distance between two action chunks, MBR chooses:

$$a_{t:t+H-1}^{\text{MBR}} = \underset{a_{t:t+H-1} \in \mathcal{A}}{\operatorname{argmin}} \mathbb{E}_{a'_{t:t+H-1} \sim \pi_\theta} [d(a_{t:t+H-1}, a'_{t:t+H-1})]. \quad (1)$$

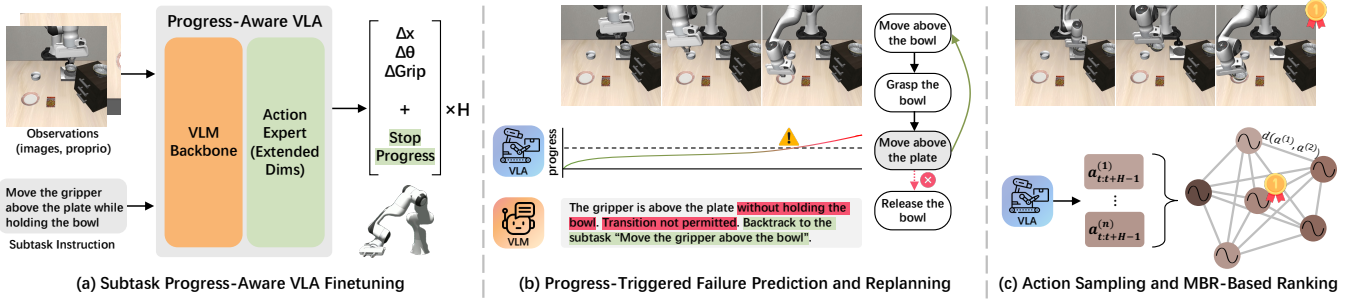


Fig. 3: **CycleVLA**. (a) A finetuning pipeline that equips a VLA with subtask-level stop and progress prediction via extended action expert dimension and augmented subtask-decomposed training data. (b) At inference, predicted progress triggers a VLM-based failure predictor and planner, which decides whether to transit to the next subtask or backtrack, and selects the subtask to backtrack to. (c) After backtracking, the VLA retries execution using test-time scaling via MBR decoding to improve success. Please see Appendices C and F for MBR implementation details and VLM exact prompts.

We approximate the expectation via Monte Carlo using the hypothesis set \mathcal{A} sampled from the policy $\pi_\theta(\cdot | o_t, g_k)$:

$$\mathcal{L}(a_{t:t+H-1}) = \frac{1}{N} \sum_{n=1}^N d(a_{t:t+H-1}, a_{t:t+H-1}^{(n)}), \quad (2)$$

where \mathcal{L} is the estimated Bayesian risk of an action chunk, yielding the sampling-based N -by- N MBR objective [34]:

$$a_{t:t+H-1}^{\text{MBR}} = \underset{a_{t:t+H-1} \in \mathcal{A}}{\operatorname{argmin}} \mathcal{L}(a_{t:t+H-1}). \quad (3)$$

We instantiate d using distance in predicted end-effector motion. For each sampled hypothesis $a_{t:t+H-1}^{(n)}$, we accumulate translational and rotational deltas to obtain a predicted trajectory, represented by a feature vector $\phi(a_{t:t+H-1}^{(n)}) \in \mathbb{R}^{6H}$ containing position (x, y, z) and orientation (u, v, w) at each step. MBR selects the consensus trajectory:

$$a_{t:t+H-1}^{\text{MBR}} = \underset{a^{(i)} \in \mathcal{A}}{\operatorname{argmin}} \frac{1}{N} \sum_{j=1}^N d(\phi(a_{t:t+H-1}^{(i)}), \phi(a_{t:t+H-1}^{(j)})), \quad (4)$$

which minimizes the average pairwise distance over the $N \times N$ distance matrix, favoring trajectories in high-density regions of the policy output space.

Overall Inference Procedure. We summarize the complete CycleVLA inference procedure in Alg. 1. The algorithm alternates between two phases per subtask: monitoring progress until the VLM check is triggered, then completing execution until the stop signal confirms subtask termination.

V. EXPERIMENTS AND ANALYSIS

We conduct experiments to answer the following questions: 1) To what extent does our proactive self-correcting VLA improve downstream task success rates, and how many failed trajectories can it recover compared to a monolithic VLA, even with under-trained VLAs? 2) How much does test-time scaling via MBR decoding contribute to performance gains in VLA inference? 3) What is the impact of each component on inference efficiency and overall effectiveness?

Algorithm 1 CycleVLA Inference

Require: Task instruction g , VLA policy π_θ , VLM \mathcal{V} , progress threshold τ_p , action chunk size H , samples N , max retries R , timeout T_{\max}

Ensure: Episode success / failure

- 1: Decompose g into subtask list $G = (g_1, \dots, g_K)$ by \mathcal{V}
- 2: $k \leftarrow 1$; $t \leftarrow 0$; phase \leftarrow MONITOR; $\mathcal{Q} \leftarrow \emptyset$; $r_{1:K} \leftarrow 0$
- 3: **while** $k \leq K$ **and** $t < T_{\max}$ **do**
- 4: Observe o_t
- 5: **if** $\mathcal{Q} = \emptyset$ **then**
- 6: Sample chunk $a_{t:t+H-1} \sim \pi_\theta(\cdot | o_t, g_k)$ and push into \mathcal{Q}
- 7: **end if**
- 8: Pop $a_t \in \mathcal{Q}$ and parse $a_t = (\tilde{a}_t, s_t, p_t)$ with $\tilde{a}_t \in \mathbb{R}^7$
- 9: Execute \tilde{a}_t ; observe o_{t+1} ; $t \leftarrow t + 1$
- 10: **if** episode succeeds **then**
- 11: **return** success
- 12: **end if**
- 13: **if** phase = MONITOR **and** CONFIRM($p_t \geq \tau_p$) **then**
- 14: $(j, \text{dec}) \leftarrow \mathcal{V}(o_t, g_k, G)$, $\text{dec} \in \{\text{transit}, \text{backtrack}\}$
- 15: **if** dec = backtrack **and** $r_j < R$ **then**
- 16: $r_j \leftarrow r_j + 1$
- 17: Restore robot to start of g_j via reverse execution; $\mathcal{Q} \leftarrow \emptyset$
- 18: Observe o_t
- 19: Sample $\mathcal{A} = \{a_{t:t+H-1}^{(n)}\}_{n=1}^N$ with $a_{t:t+H-1}^{(n)} \sim \pi_\theta(\cdot | o_t, g_j)$
- 20: Select $a_{t:t+H-1}^{\text{MBR}}$ via Eq. (4) and set $\mathcal{Q} \leftarrow a_{t:t+H-1}^{\text{MBR}}$
- 21: $k \leftarrow j$; phase \leftarrow MONITOR
- 22: **else**
- 23: phase \leftarrow COMPLETE
- 24: **end if**
- 25: **else if** phase = COMPLETE **and** CONFIRM($s_t = 1$) **then**
- 26: $k \leftarrow k + 1$; phase \leftarrow MONITOR; $\mathcal{Q} \leftarrow \emptyset$
- 27: **end if**
- 28: **end while**
- 29: **return** failure

A. Implementation Details

Subtask Decomposition. We use GPT-4.1 [65] (temperature 0.2) to propose subtasks and infer their timestamp boundaries. The last action step of each subtask is oversampled by a factor of 8. Please see Appendix B for more details.

Training and Inference. The VLA backbone is OpenVLA [66] with a diffusion-based action expert. Stochastic sampling is achieved by varying random seeds, which changes the noise sampling in the diffusion process. All models are trained on 4 NVIDIA A100 GPUs (40GB VRAM) and evaluated on 1 NVIDIA A10 GPU (24GB VRAM) unless

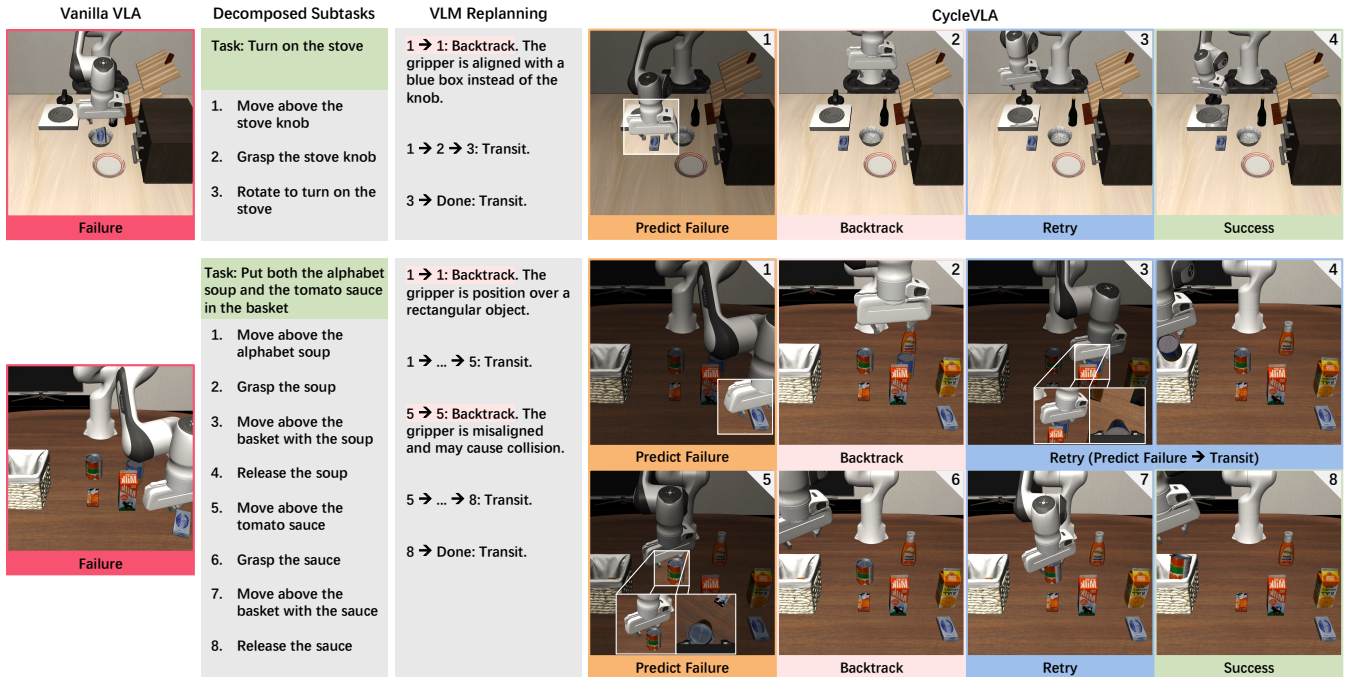


Fig. 4: **Qualitative examples of CycleVLA.** CycleVLA performs multiple cycles of failure prediction, backtracking, and retry within a single long-horizon task, correcting errors across subtasks and achieving successful completion. More examples can be found in Appendix D.

otherwise specified. We use GPT-5.2 [67] (temperature 1.0) as the VLM-based failure predictor and planner, queried when subtask progress reaches $\tau_p = 0.9$. For MBR decoding, we use an L_2 distance metric (d) with $N = 8$ sampled hypotheses. Please see Appendices C and D for more details.

B. Evaluation on Simulation Benchmarks

Setup. We evaluate on LIBERO [68] using four task suites: Spatial, Object, Goal, and Long, following OpenVLA [13] for data preprocessing and evaluation. Each suite contains 10 tasks, evaluated over 50 rollouts with 3 random seeds. For finetuning, we follow [69]–[71] and train a single model jointly on data from all four suites, rather than training separate models per suite as in [13], [66], [72]. Joint training increases task and scene diversity and thus presents a more challenging learning setting. We report results alongside baseline numbers regardless of the finetuning paradigm.

Task Performance. As shown in Table. I, prior methods often achieve lower success rates on LIBERO-Long due to its challenging long-horizon nature. CycleVLA achieves notably higher success rates on this task suite by predicting failures at subtask boundaries and backtracking to retry. This self-correcting mechanism is particularly effective for long-horizon tasks, where errors tend to accumulate across subtasks.

Effectiveness on Under-Trained VLAs. In practice, due to computational constraints or the high difficulty of certain robotic tasks, some VLAs may be under-trained. We investigate whether CycleVLA remains effective across VLAs with varying capacities. We select two intermediate checkpoints (trained after 200K and 350K steps) alongside our final 500K checkpoint, and compare performance before and after

TABLE I: **LIBERO task performance** (success rates \uparrow).

Method	Spatial	Object	Goal	Long	Average
Diffusion Policy [73]	78.3	82.5	68.3	50.5	72.4
Octo-Base [74]	78.9	85.7	84.6	51.1	75.1
OpenVLA [13]	84.7	88.4	79.2	53.7	76.5
TraceVLA [69]	84.6	85.2	75.1	54.1	74.8
SpatialVLA [75]	88.2	89.9	78.6	55.5	78.1
ThinkAct [70]	88.3	91.4	87.1	70.9	84.4
CoT-VLA [46]	87.5	91.6	87.6	69.0	81.1
FPC-VLA [71]	87.0	92.0	86.2	82.2	86.9
GR00T N1 [15]	94.4	97.6	93.0	90.6	93.9
CycleVLA	97.6	98.1	91.7	93.6	95.3

applying failure correction. In the no-correction setting, the policy naturally progresses to the next subtask when a stop signal is triggered. Results in Table. II show that CycleVLA provides consistent gains across all checkpoints. Notably, CycleVLA bridges the gap between model sizes: the 200K and 350K checkpoints with CycleVLA approach the performance of the 350K and 500K checkpoints without it.

Qualitative Results. we show qualitative examples of CycleVLA in Fig. 4 on tasks with varying horizons.

C. Analysis of MBR Decoding

Setup. We evaluate MBR decoding as a test-time scaling strategy for VLAs by measuring its ability to select successful action chunks from multiple stochastic hypotheses. For a given base VLA and MBR hyperparameter setting, results are averaged over 2 randomly selected tasks from each LIBERO task suite (8 tasks in total).

For each task, we evaluate on $E = 200$ episodes. In each episode, we execute the VLA for N stochastic trials, following

TABLE II: **Recovery performance on under-trained VLAs.** Success rates \uparrow on LIBERO with and without failure correction (FC).

Method	Spatial		Object		Goal		Long		Average	
	w/o FC	w/ FC	w/o FC	w/ FC	w/o FC	w/ FC	w/o FC	w/ FC	w/o FC	w/ FC
CycleVLA-200K	84.7	89.1 (+4.4)	82.0	90.2 (+8.2)	63.6	74.2 (+10.6)	62.3	66.5 (+4.2)	73.2	80.0 (+6.8)
CycleVLA-350K	88.4	94.8 (+6.4)	93.8	97.5 (+3.7)	72.6	79.4 (+6.8)	77.9	85.3 (+7.4)	83.2	89.2 (+6.0)
CycleVLA-500K	91.1	97.6 (+6.5)	95.3	98.1 (+2.8)	86.5	91.7 (+5.2)	84.4	93.6 (+9.2)	89.3	95.3 (+6.0)

TABLE III: **Effect of number of hypotheses on MBR performance.** Estimated success probability ($P_{\text{succ}} \uparrow$). SR denotes the average success rate of the base VLA on LIBERO without failure correction.

Method	SR	4		8		16		32		64	
		random	MBR	random	MBR	random	MBR	random	MBR	random	MBR
CycleVLA-200K	73.2	72.9	78.2 (+5.3)	71.7	78.5 (+6.8)	71.9	81.2 (+9.3)	72.2	79.7 (+7.5)	72.3	79.7 (+7.4)
CycleVLA-350K	83.2	80.5	88.0 (+7.5)	80.3	90.2 (+9.9)	80.2	91.3 (+11.1)	80.4	92.3 (+11.9)	80.7	92.2 (+11.5)
CycleVLA-500K	89.3	90.8	94.1 (+3.3)	90.2	95.5 (+5.3)	91.1	95.7 (+4.6)	90.7	95.7 (+5.0)	90.4	95.6 (+5.2)

the same execution protocol as the no-correction setting. We record the resulting trajectories and their success outcomes, and treat these N executions as hypotheses. For each episode e , we define the set of decision steps (chunk boundaries) as $\mathcal{T}_e = \{0, H, 2H, \dots\}$, where H is the action chunk size. Each recorded trajectory is divided accordingly, yielding a temporally aligned set of chunk hypotheses $\{a_{t:t+H-1}^{(n)}\}_{n=1}^N$ at each step $t \in \mathcal{T}_e$.

At each step $t \in \mathcal{T}_e$, we compare two selection strategies over the same hypothesis set: 1) MBR decoding using Eq. (4), and 2) random selection of a single hypothesis. Let $z_{e,t}^{(n)} \in \{0, 1\}$ indicate whether hypothesis n is successful at decision step t in episode e (inherited from the recorded rollout). For a selection method $m \in \{\text{MBR}, \text{RANDOM}\}$, let $\hat{n}_{e,t}^{(m)} \in \{1, \dots, N\}$ denote the selected hypothesis index at step t . For each episode, we compute a score by averaging the success of the selected chunks over all decision steps. The final estimated success probability is then obtained by averaging over episodes:

$$P_{\text{succ}}^{(m)} = \frac{1}{E} \sum_{e=1}^E \left(\frac{1}{|\mathcal{T}_e|} \sum_{t \in \mathcal{T}_e} z_{e,t}^{(\hat{n}_{e,t}^{(m)})} \right). \quad (5)$$

This metric estimates the probability of choosing a successful action chunk from N sampled hypotheses, averaged across trajectory timestamps and repeated runs.

Number of Hypotheses. We study the effect of the number of hypotheses by varying $N \in \{4, 8, 16, 32, 64\}$, using an L_2 distance metric. Increasing N generally improves MBR performance by better approximating expected risk (Eq.(1)), but with diminishing returns and higher computational cost due to increased sampling and pairwise distance evaluation. As shown in Table. III, most gains are achieved when

increasing N from 4 to 8, while improvements plateau beyond $N = 16$, with similar performance for $N = 32$ and 64.

Without MBR decoding, random selection achieves a success probability similar to the base VLA because it samples action chunks directly from the model’s stochastic output distribution. Averaging performance across chunks, episodes, and tasks therefore reflects the marginal behavior of the underlying policy, without introducing any bias toward higher-quality candidates.

In contrast, MBR decoding consistently improves success probability across VLAs of varying capability, with larger gains observed for under-trained models (200K and 350K steps) compared to the fully trained 500K model. This trend aligns with observations in LLMs that weaker models benefit more from MBR-style selection [76], as stronger models tend to produce more self-consistent candidates, reducing the marginal benefit of hypothesis selection.

Choice of Distance Metric. We analyze the sensitivity of MBR decoding to the choice of distance metric d used in the pairwise distance computation (Eq. (4)). We evaluate common metrics, including L_1 , L_2 , Chebyshev (L_∞), cosine similarity (\cos), and correlation (r), with the number of hypotheses fixed to $N = 8$. As shown in Table. IV, L_2 consistently achieves the best performance across all VLAs, followed by L_1 , while \cos and r yield the smallest improvements. We hypothesize this is because translational components are dense along the trajectory, whereas rotational components are relatively sparse, with limited rotation at many timesteps. Distance-based metrics such as L_1 and L_2 therefore better capture magnitude differences in action sequences, while \cos and r emphasize directional agreement.

TABLE IV: **Effect of distance metric on MBR performance.** Estimated success probability ($P_{\text{succ}} \uparrow$). SR denotes the average success rate of the base VLA on LIBERO without failure correction.

Method	SR	Random	MBR- L_1	MBR- L_2	MBR- L_∞	MBR-cos	MBR- r
CycleVLA-200K	73.2	71.7	78.7 (+7.0)	78.5 (+6.8)	77.8 (+6.1)	74.1 (+2.4)	73.5 (+1.8)
CycleVLA-350K	83.2	80.3	89.7 (+9.4)	90.2 (+9.9)	88.2 (+7.9)	87.5 (+7.2)	86.9 (+6.6)
CycleVLA-500K	89.3	90.2	94.7 (+4.5)	95.5 (+5.3)	94.3 (+4.1)	94.4 (+4.2)	94.8 (+4.6)

TABLE V: **Runtime analysis of test-time scaling on LIBERO.** End-to-end runtime in seconds (s ↓) for each component on different GPUs. Percentages indicate share of total inference time.

GPU	VLM	Action Rollout	Action Sampling	MBR	Backtrack	Total
A10	12.9 (6.0%)	147.6 (68.6%)	47.9 (22.2%)	0.003 (<0.1%)	6.9 (3.2%)	215.3
A100	15.3 (19.9%)	44.7 (58.1%)	11.9 (15.5%)	0.002 (<0.1%)	5.0 (6.5%)	76.9

D. Runtime Analysis of Test-Time Scaling

We analyze the contribution of each component in CycleVLA to inference-time overhead under test-time scaling. For each task episode, we record the runtime of: 1) VLM failure prediction and planning (OpenAI API call, Tier-5 user), 2) VLA action inference and robot execution, 3) action sampling after backtracking, 4) MBR pairwise distance computation, and 5) backtracking execution. We compare runtime on NVIDIA A10 and A100 GPUs. From Table. V, standard action rollout remains the dominant bottleneck, while test-time scaling in CycleVLA increases overall runtime by $\sim 30\%$. With stronger GPUs, the relative proportion of VLM API latency increases, as action inference becomes faster. We consider this overhead acceptable, as test-time scaling methods in LLMs typically incur linear or near-linear runtime increases with the number of samples [59], [77].

E. Ablation Studies

We evaluate the effectiveness of each component by removing or replacing it with an alternative design. **1) Removing MBR decoding:** After backtracking, MBR decoding is replaced with random hypothesis selection. **2) Changing VLM backbone:** We replace GPT-5.2 [67] with the smaller LLaMA-3.2-11B [24] to assess robustness. **3) Removing stop signal and last-action oversampling:** We remove stop signal prediction and last-action oversampling during finetuning, reducing the action to $a_t = [\Delta x_t, \Delta y_t, \Delta z_t, \Delta u_t, \Delta v_t, \Delta w_t, \gamma_t, p_t]^\top \in \mathbb{R}^8$, and consider a subtask complete when $p_t \geq 0.95$ at inference. **4) Always-on MBR decoding (upper bound):** MBR decoding is applied at initial execution and every high-progress subtask transitions, without using the VLM to decide if to transit or backtrack. **5) Predicted failure cutoff (lower bound):** When the VLM predicts a potential failure, the episode is immediately terminated and counted as a failure. In principle, the resulting success rate should match that of the VLA without failure correction (Table. II), and thus serves to evaluate the robustness of VLM failure prediction.

From Table VI, removing MBR leads to a moderate drop in success rate, as retrying up to R times (Alg. 1) already provides partial robustness at the cost of runtime. Using LLaMA-3.2-11B reduces both success rate and runtime, as local inference is faster and we observe that LLaMA-3.2-11B more frequently chooses to transit rather than backtrack, leading to less action sampling and MBR computation. Removing stop signal and last-frame oversampling reduces both metrics due to spurious high-progress predictions causing premature termination. The always-on MBR variant achieves higher success but incurs substantially higher runtime from

TABLE VI: **Ablation study on LIBERO.** Averaged success rate (SR) and inference time after removing individual components. LAO = last-action oversampling; UB = upper bound; LB = lower bound.

Method	SR ↑	Time (s ↓)
CycleVLA (w/o MBR)	92.5	302.4
CycleVLA (alt. VLM)	92.8	172.6
CycleVLA (w/o stop + LAO)	91.1	186.8
CycleVLA (always-on MBR, UB)	96.9	464.3
CycleVLA (pred. failure cutoff, LB)	79.7	110.2
CycleVLA (main)	95.3	215.3

MBR computation at every transition. Finally, terminating upon VLM-predicted failure causes a modest $\sim 10\%$ drop, illustrating LLM/VLM sycophancy [78]–[81]: when asked to predict failure, the VLM tends to confirm this assumption.

VI. CONCLUSION AND DISCUSSION

We introduce **CycleVLA**, a system that equips VLAs with proactive self-correction, the capability to anticipate incipient failures and recover before execution collapses. We see our work as an early investigation into granting VLAs such abilities and exploring test-time scaling for VLAs. CycleVLA relies on an external VLM for failure prediction and replanning, and an explicit backtracking mechanism. Future work may investigate integrating these capabilities directly into VLAs to enable end-to-end failure reasoning and learned recovery behaviors, as well as tailored test-time scaling strategies for VLAs.

Limitations. Our backtracking mechanism assumes reversible state transitions, which may not hold in highly dynamic or irreversible environments. Test-time scaling via MBR decoding requires multiple forward passes, which increases inference time and can be further optimized for contact-rich tasks requiring high control frequencies. Experiments on real robot hardware to be added in the near future.

REFERENCES

- [1] A. Xie, F. Tajwar, A. Sharma, and C. Finn, "When to ask for help: Proactive interventions in autonomous reinforcement learning," in *Advances in Neural Information Processing Systems*, 2022.
- [2] A. Farid, D. Snyder, A. Z. Ren, and A. Majumdar, "Failure prediction with statistical guarantees for vision-based robot control," in *Robotics: Science and Systems*, 2022.
- [3] Y. Du, K. Konyushkova, M. Denil, A. Raju, J. Landon, F. Hill, N. de Freitas, and S. Cabi, "Vision-language models as success detectors," in *Conference on Lifelong Learning Agents*, 2023.
- [4] C. Gokmen, D. Ho, and M. Khansari, "Asking for help: Failure prediction in behavioral cloning through value approximation," in *International Conference on Robotics and Automation*, 2023.
- [5] C. Agia, R. Sinha, J. Yang, Z. Cao, R. Antonova, M. Pavone, and J. Bohg, "Unpacking failure modes of generative policies: Runtime monitoring of consistency and progress," in *Conference on Robot Learning*, 2024.
- [6] R. Ramrakhya, M. Chang, X. Puig, R. Desai, Z. Kira, and R. Mottaghi, "Grounding multimodal llms to embodied agents that ask for help with reinforcement learning," *arXiv preprint arXiv:2504.00907*, 2025.
- [7] N. Sun, Y. Li, C. Wang, H. Li, and H. Liu, "Collabvla: Self-reflective vision-language-action model dreaming together with human," *arXiv preprint arXiv:2509.14889*, 2025.
- [8] Q. Gu, Y. Ju, S. Sun, I. Gilitschenski, H. Nishimura, M. Itkina, and F. Shkurti, "SAFE: multitask failure detection for vision-language-action models," in *Advances in Neural Information Processing Systems*, 2025.
- [9] Z. Liu, A. Bahety, and S. Song, "REFLECT: summarizing robot experiences for failure explanation and correction," in *Conference on Robot Learning*, 2023.
- [10] J. Duan, W. Pumacay, N. Kumar, Y. R. Wang, S. Tian, W. Yuan, R. Krishna, D. Fox, A. Mandlekar, and Y. Guo, "AHA: A vision-language-model for detecting and reasoning over failures in robotic manipulation," in *International Conference on Learning Representations*, 2025.
- [11] K. Lu, C. Ma, C. Hori, and D. Romeres, "KitchenVLA: Iterative vision-language corrections for robotic execution of human tasks," in *International Conference on Robotics and Automation Workshop on Safely Leveraging Vision-Language Foundation Models in Robotics*, 2025.
- [12] M. S. Sakib and Y. Sun, "STAR: A foundation model-driven framework for robust task planning and failure recovery in robotic systems," *arXiv preprint arXiv:2503.06060*, 2025.
- [13] M. J. Kim, K. Pertsch, S. Karamcheti, T. Xiao, A. Balakrishna, S. Nair, R. Rafailov, E. P. Foster, P. R. Sanketi, Q. Vuong, T. Kollar, B. Burchfiel, R. Tedrake, D. Sadigh, S. Levine, P. Liang, and C. Finn, "Openvla: An open-source vision-language-action model," in *Conference on Robot Learning*, 2024.
- [14] K. Black, N. Brown, D. Driess, A. Esmail, M. Equi, C. Finn, N. Fusai, L. Groom, K. Hausman, B. Ichter, S. Jakubczak, T. Jones, L. Ke, S. Levine, A. Li-Bell, M. Mothukuri, S. Nair, K. Pertsch, L. X. Shi, J. Tanner, Q. Vuong, A. Walling, H. Wang, and U. Zhilinsky, " π_0 : A vision-language-action flow model for general robot control," *arXiv preprint arXiv:2410.24164*, 2024.
- [15] J. Bjorck, F. Castañeda, N. Cherniadev, X. Da, R. Ding, L. Fan, Y. Fang, D. Fox, F. Hu, S. Huang, J. Jang, Z. Jiang, J. Kautz, K. Kundalia, L. Lao, Z. Li, Z. Lin, K. Lin, G. Liu, E. Llopart, L. Magne, A. Mandlekar, A. Narayan, S. Nasiriany, S. Reed, Y. L. Tan, G. Wang, Z. Wang, J. Wang, Q. Wang, J. Xiang, Y. Xie, Y. Xu, Z. Xu, S. Ye, Z. Yu, A. Zhang, H. Zhang, Y. Zhao, R. Zheng, and Y. Zhu, "GR00T N1: an open foundation model for generalist humanoid robots," *arXiv preprint arXiv:2503.14734*, 2025.
- [16] V. Myers, C. Zheng, O. Mees, K. Fang, and S. Levine, "Policy adaptation via language optimization: Decomposing tasks for few-shot imitation," in *Conference on Robot Learning*, 2024.
- [17] P. Intelligence, K. Black, N. Brown, J. Darpinian, K. Dhabalia, D. Driess, A. Esmail, M. Equi, C. Finn, N. Fusai, M. Y. Galliker, D. Ghosh, L. Groom, K. Hausman, B. Ichter, S. Jakubczak, T. Jones, L. Ke, D. LeBlanc, S. Levine, A. Li-Bell, M. Mothukuri, S. Nair, K. Pertsch, A. Z. Ren, L. X. Shi, L. Smith, J. T. Springenberg, K. Stachowicz, J. Tanner, Q. Vuong, H. Walke, A. Walling, H. Wang, L. Yu, and U. Zhilinsky, " $\pi_{0.5}$: a vision-language-action model with open-world generalization," *arXiv preprint arXiv:2504.16054*, 2025.
- [18] L. X. Shi, B. Ichter, M. R. Equi, L. Ke, K. Pertsch, Q. Vuong, J. Tanner, A. Walling, H. Wang, N. Fusai, A. Li-Bell, D. Driess, L. Groom, S. Levine, and C. Finn, "Hi robot: Open-ended instruction following with hierarchical vision-language-action models," in *International Conference on Machine Learning*, 2025.
- [19] R. Yang, Z. An, L. Zhou, and Y. Feng, "Seqvla: Sequential task execution for long-horizon manipulation with completion-aware vision-language-action model," *arXiv preprint arXiv:2509.14138*, 2025.
- [20] Y. Fan, P. Ding, S. Bai, X. Tong, Y. Zhu, H. Lu, F. Dai, W. Zhao, Y. Liu, S. Huang, Z. Fan, B. Chen, and D. Wang, "Long-vla: Unleashing long-horizon capability of vision language action model for robot manipulation," in *Conference on Robot Learning*, 2025.
- [21] L. Ke, X. Li, Y. Bisk, A. Holtzman, Z. Gan, J. Liu, J. Gao, Y. Choi, and S. Srinivasa, "Tactical rewind: Self-correction via backtracking in vision-and-language navigation," in *Conference on Computer Vision and Pattern Recognition*, 2019.
- [22] X. Shi, Z. Li, W. Lyu, J. Xia, F. Dayoub, Y. Qiao, and Q. Wu, "Smartway: Enhanced waypoint prediction and backtracking for zero-shot vision-and-language navigation," in *International Conference on Intelligent Robots and Systems*, 2025.
- [23] M. Du, A. Khazatsky, T. Gerstenberg, and C. Finn, "To err is robotic: Rapid value-based trial-and-error during deployment," *arXiv preprint arXiv:2406.15917*, 2024.
- [24] T. L. . Team, "The llama 3 herd of models," *arXiv preprint arXiv:2407.21783*, 2024.
- [25] T. B. Brown, B. Mann, N. Ryder, M. Subbiah, J. Kaplan, P. Dhariwal, A. Neelakantan, P. Shyam, G. Sastry, A. Askell, S. Agarwal, A. Herbert-Voss, G. Krueger, T. Henighan, R. Child, A. Ramesh, D. M. Ziegler, J. Wu, C. Winter, C. Hesse, M. Chen, E. Sigler, M. Litwin, S. Gray, B. Chess, J. Clark, C. Berner, S. McCandlish, A. Radford, I. Sutskever, and D. Amodei, "Language models are few-shot learners," in *Advances in Neural Information Processing Systems*, 2020.
- [26] C. Ma, K. Lu, T.-Y. Cheng, N. Trigoni, and A. Markham, "Spatialpin: Enhancing spatial reasoning capabilities of vision-language models through prompting and interacting 3d priors," in *Neural Information Processing Systems*, 2024.
- [27] F. Yang, C. Ma, J. Zhang, J. Zhu, W. Yuan, and A. Owens, "Touch and go: Learning from human-collected vision and touch," *Advances in Neural Information Processing Systems*, 2022.
- [28] H. Liu, C. Li, Y. Li, and Y. J. Lee, "Improved baselines with visual instruction tuning," in *Conference on Computer Vision and Pattern Recognition*, 2024.
- [29] S. Kumar and W. J. Byrne, "Minimum bayes-risk decoding for statistical machine translation," in *Human Language Technology Conference of the North American Chapter of the Association for Computational Linguistics*, 2004.
- [30] O. X.-E. Collaboration, "Open x-embodiment: Robotic learning datasets and RT-X models : Open x-embodiment collaboration," in *International Conference on Robotics and Automation*, 2024.
- [31] S. Liu, L. Wu, B. Li, H. Tan, H. Chen, Z. Wang, K. Xu, H. Su, and J. Zhu, "RDT-1B: a diffusion foundation model for bimanual manipulation," in *International Conference on Learning Representations*, 2025.
- [32] J. Kwok, C. Agia, R. Sinha, M. Foutter, S. Li, I. Stoica, A. Mirhoseini, and M. Pavone, "Robomonkey: Scaling test-time sampling and verification for vision-language-action models," in *Conference on Robot Learning*, 2025.
- [33] M. Dai, L. Liu, Y. Bai, Y. Liu, Z. Wang, R. SU, C. Chen, L. Lin, and X. Wu, "Rover: Robot reward model as test-time verifier for vision-language-action model," *arXiv preprint arXiv:2510.10975*, 2025.
- [34] B. Eikema and W. Aziz, "Sampling-based approximations to minimum bayes risk decoding for neural machine translation," in *Empirical Methods in Natural Language Processing*, 2022.
- [35] J. Chen, G. Yang, W. Lin, J. Mei, and B. Byrne, "On extending direct preference optimization to accommodate ties," in *Advances in Neural Information Processing Systems*, 2025.
- [36] G. Yang, J. Chen, W. Lin, and B. Byrne, "Direct preference optimization for neural machine translation with minimum bayes risk decoding," in *Conference of the North American Chapter of the Association for Computational Linguistics*, 2024.
- [37] C. Xu, T. K. Nguyen, E. Dixon, C. Rodriguez, P. T. Miller, R. Lee, P. Shah, R. Ambrus, H. Nishimura, and M. Itkina, "Can we detect failures without failure data? uncertainty-aware runtime failure detection for imitation learning policies," *arXiv preprint arXiv:2503.08558*, 2025.

- [38] F. Yang and C. Ma, "Sparse and complete latent organization for geospatial semantic segmentation," in *Conference on Computer Vision and Pattern Recognition*, 2022.
- [39] J. Wong, A. Tung, A. Kurenkov, A. Mandlekar, L. Fei-Fei, S. Savarese, and R. Martín-Martín, "Error-aware imitation learning from teleoperation data for mobile manipulation," in *Conference on Robot Learning*, 2021.
- [40] H. Liu, S. Dass, R. Martín-Martín, and Y. Zhu, "Model-based runtime monitoring with interactive imitation learning," in *International Conference on Robotics and Automation*, 2024.
- [41] R. Sinha, A. Elhafi, C. Agia, M. Foutter, E. Schmerling, and M. Pavone, "Real-time anomaly detection and reactive planning with large language models," in *Robotics: Science and Systems*, 2024.
- [42] Y. Guo, Y. Wang, L. Zha, and J. Chen, "Doremi: Grounding language model by detecting and recovering from plan-execution misalignment," in *International Conference on Intelligent Robots and Systems*, 2024.
- [43] C. Li, J. Liu, G. Wang, X. Li, S. Chen, L. Heng, C. Xiong, J. Ge, R. Zhang, K. Zhou, and S. Zhang, "A self-correcting vision-language-action model for fast and slow system manipulation," *arXiv preprint arXiv:2405.17418*, 2025.
- [44] C. Ma, K. Lu, R. Desai, X. Puig, A. Markham, and N. Trigoni, "Coopera: Continual open-ended human-robot assistance," in *Advances in Neural Information Processing Systems*, 2025.
- [45] H. Liu, Y. Zhang, V. Betala, E. Zhang, J. Liu, C. Ding, and Y. Zhu, "Multi-task interactive robot fleet learning with visual world models," in *Conference on Robot Learning*, 2024.
- [46] Q. Zhao, Y. Lu, M. J. Kim, Z. Fu, Z. Zhang, Y. Wu, Z. Li, Q. Ma, S. Han, C. Finn, A. Handa, T. Lin, G. Wetzstein, M. Liu, and D. Xiang, "Cot-vla: Visual chain-of-thought reasoning for vision-language-action models," in *Conference on Computer Vision and Pattern Recognition*, 2025.
- [47] Y. Feng, J. Han, Z. Yang, X. Yue, S. Levine, and J. Luo, "Reflective planning: Vision-language models for multi-stage long-horizon robotic manipulation," *arXiv preprint arXiv:2502.16707*, 2025.
- [48] M. Assran, A. Bardes, D. Fan, Q. Garrido, R. Howes, M. Komeili, M. J. Muckley, A. Rizvi, C. Roberts, K. Sinha, A. Zholus, S. Arnaud, A. Gejji, A. Martin, F. R. Hogan, D. Dugas, P. Bojanowski, V. Khalidov, P. Labatut, F. Massa, M. Szafraniec, K. Krishnakumar, Y. Li, X. Ma, S. Chandar, F. Meier, Y. LeCun, M. Rabbat, and N. Ballas, "V-JEPA 2: Self-supervised video models enable understanding, prediction and planning," *arXiv preprint arXiv:2506.09985*, 2025.
- [49] J. Wen, Y. Zhu, J. Li, Z. Tang, C. Shen, and F. Feng, "Dexvla: Vision-language model with plug-in diffusion expert for general robot control," in *Conference on Robot Learning*, 2025.
- [50] M. Yan, Y. Wang, Z. Liu, and J. Li, "RDD: retrieval-based demonstration decomposer for planner alignment in long-horizon tasks," in *Advances in Neural Information Processing Systems*, 2025.
- [51] M. Zawalski, W. Chen, K. Pertsch, O. Mees, C. Finn, and S. Levine, "Robotic control via embodied chain-of-thought reasoning," in *Conference on Robot Learning*, 2024.
- [52] Z. Zhou, Y. Zhu, M. Zhu, J. Wen, N. Liu, Z. Xu, W. Meng, R. Cheng, Y. Peng, C. Shen, and F. Feng, "Chatvla: Unified multimodal understanding and robot control with vision-language-action model," in *Empirical Methods in Natural Language Processing*, 2025.
- [53] Z. Zhou, Y. Zhu, J. Wen, C. Shen, and Y. Xu, "Chatvla-2: Vision-language-action model with open-world embodied reasoning from pretrained knowledge," in *Advances in Neural Information Processing Systems*, 2025.
- [54] W. Chen, S. Belkhale, S. Mirchandani, O. Mees, D. Driess, K. Pertsch, and S. Levine, "Training strategies for efficient embodied reasoning," in *Conference on Robot Learning*, 2025.
- [55] NVIDIA, "World simulation with video foundation models for physical ai," *arXiv preprint arXiv:2511.00062*, 2025.
- [56] A. J. Hancock, A. Z. Ren, and A. Majumdar, "Run-time observation interventions make vision-language-action models more visually robust," in *International Conference on Robotics and Automation*, 2025.
- [57] E. Hannus, M. Malin, T. N. Le, and V. Kyrki, "IA-VLA: input augmentation for vision-language-action models in settings with semantically complex tasks," *arXiv preprint arXiv:2509.24768*, 2025.
- [58] A. Bar, Y. Gandelsman, T. Darrell, A. Globerson, and A. A. Efros, "Visual prompting via image inpainting," in *Advances in Neural Information Processing Systems*, 2022.
- [59] C. Snell, J. Lee, K. Xu, and A. Kumar, "Scaling LLM test-time compute optimally can be more effective than scaling model parameters," in *International Conference on Learning Representations*, 2025.
- [60] DeepSeek-AI, "Deepseek-r1: Incentivizing reasoning capability in llms via reinforcement learning," *arXiv preprint arXiv:2501.12948*, 2025.
- [61] O. AI, "Introducing openai o3 and o4-mini," <https://openai.com/index/introducing-o3-and-o4-mini/>, 2025.
- [62] M. Nakamoto, O. Mees, A. Kumar, and S. Levine, "Steering your generalists: Improving robotic foundation models via value guidance," in *Conference on Robot Learning*, 2024.
- [63] J. Zhang, K. Wang, R. Xu, G. Zhou, Y. Hong, X. Fang, Q. Wu, Z. Zhang, and H. Wang, "Navid: Video-based VLM plans the next step for vision-and-language navigation," in *Robotics: Science and Systems*, 2024.
- [64] J. Wei, X. Wang, D. Schuurmans, M. Bosma, B. Ichter, F. Xia, E. H. Chi, Q. V. Le, and D. Zhou, "Chain-of-thought prompting elicits reasoning in large language models," in *Advances in Neural Information Processing Systems*, 2022.
- [65] O. AI, "Introducing gpt-4.1 in the api," <https://openai.com/index/gpt-4-1/>, 2025.
- [66] M. J. Kim, C. Finn, and P. Liang, "Fine-tuning vision-language-action models: Optimizing speed and success," in *Robotics: Science and Systems*, 2025.
- [67] O. AI, "Introducing gpt-5.2," <https://openai.com/index/introducing-gpt-5-2/>, 2025.
- [68] B. Liu, Y. Zhu, C. Gao, Y. Feng, Q. Liu, Y. Zhu, and P. Stone, "LIBERO: benchmarking knowledge transfer for lifelong robot learning," in *Advances in Neural Information Processing Systems*, 2023.
- [69] R. Zheng, Y. Liang, S. Huang, J. Gao, H. D. III, A. Kolobov, F. Huang, and J. Yang, "Tracevla: Visual trace prompting enhances spatial-temporal awareness for generalist robotic policies," in *International Conference on Learning Representations*, 2025.
- [70] C.-P. Huang, Y.-H. Wu, M.-H. Chen, Y.-C. F. Wang, and F.-E. Yang, "Thinkact: Vision-language-action reasoning via reinforced visual latent planning," in *Advances in Neural Information Processing Systems*, 2025.
- [71] Y. Yang, Z. Duan, T. Xie, F. Cao, P. Shen, P. Song, P. Jin, G. Sun, S. Xu, Y. You, and J. Liu, "FPC-VLA: A vision-language-action framework with a supervisor for failure prediction and correction," *arXiv preprint arXiv:2509.04018*, 2025.
- [72] W. Li, R. Zhang, R. Shao, J. He, and L. Nie, "Cogvla: Cognition-aligned vision-language-action model via instruction-driven routing & sparsification," in *Advances in Neural Information Processing Systems*, 2025.
- [73] C. Chi, S. Feng, Y. Du, Z. Xu, E. Cousineau, B. Burchfiel, and S. Song, "Diffusion policy: Visuomotor policy learning via action diffusion," in *Robotics: Science and Systems*, 2023.
- [74] D. Ghosh, H. R. Walke, K. Pertsch, K. Black, O. Mees, S. Dasari, J. Hejna, T. Kreiman, C. Xu, J. Luo, Y. L. Tan, L. Y. Chen, Q. Vuong, T. Xiao, P. R. Sanketi, D. Sadigh, C. Finn, and S. Levine, "Octo: An open-source generalist robot policy," in *Robotics: Science and Systems*, 2024.
- [75] D. Qu, H. Song, Q. Chen, Y. Yao, X. Ye, Y. Ding, Z. Wang, J. Gu, B. Zhao, D. Wang *et al.*, "Spatialvla: Exploring spatial representations for visual-language-action model," *arXiv preprint arXiv:2501.15830*, 2025.
- [76] D. Heineman, Y. Dou, and W. Xu, "Improving minimum bayes risk decoding with multi-prompt," in *Empirical Methods in Natural Language Processing*, 2024.
- [77] H. Sun, M. Haider, R. Zhang, H. Yang, J. Qiu, M. Yin, M. Wang, P. L. Bartlett, and A. Zanette, "Fast best-of-n decoding via speculative rejection," in *Advances in Neural Information Processing Systems*, 2024.
- [78] M. Sharma, M. Tong, T. Korbak, D. Duvenaud, A. Asbell, S. R. Bowman, E. Durmus, Z. Hatfield-Dodds, S. R. Johnston, S. Kravec, T. Maxwell, S. McCandlish, K. Ndousse, O. Rausch, N. Schiefer, D. Yan, M. Zhang, and E. Perez, "Towards understanding sycophancy in language models," in *International Conference on Learning Representations*, 2024.
- [79] X. Qiu, H. Pan, W. Zhao, C. Ma, P. P. B. de Gusmao, and N. D. Lane, "Efficient vertical federated learning with secure aggregation," in *Federated Learning Systems (FLSys) Workshop@ MLSys 2023*, 2023.
- [80] X. Qiu, H. Pan, W. Zhao, C. Ma, P. P. Gusmao, and N. D. Lane, "vFedsec: Efficient secure aggregation for vertical federated learning via secure layer," *arXiv preprint arXiv:2305.16794*, 2023.
- [81] C. Ma, X. Qiu, D. Beutel, and N. Lane, "Gradient-less federated gradient boosting tree with learnable learning rates," in *Proceedings of the 3rd Workshop on Machine Learning and Systems*, 2023.

Appendix for CycleVLA

A. OVERVIEW

This Appendix includes: 1) details and human evaluation of our subtask decomposition pipeline, 2) implementation details of our density-based MBR decoding strategy, 3) additional experiments and details, and 4) prompt details for the LLM subtask decomposition and VLM failure predictor and planner.

B. DETAILS AND EVALUATION OF SUBTASK DECOMPOSITION

B.1. Movement Primitive Extraction

List of Movement Primitives. Same as ECoT [51]. Movement labels take the form:

```
move [forward/backward] [left/right] [up/down],
tilt [up/down],
rotate [clockwise/counterclockwise],
[close/open] gripper
```

Components below threshold are omitted. If no movement is detected, the label is stop.

Sliding Window Classification. Following [51], we classify movement primitives by computing the difference between robot states over a sliding window of 4 timesteps and thresholding each dimension to produce a discrete movement label.

Initial Thresholds. For LIBERO, we convert axis-angle rotation to Euler angles and normalize gripper width from two finger positions to a single value in $[0, 1]$ using max finger distance of 0.04 m. We use separate thresholds for translation, rotation, and gripper:

LIBERO: $[\tau_{\text{trans}}, \tau_{\text{rot}}, \tau_{\text{grip}}] = [0.02, 0.0075, 0.03]$

Per-Trajectory Translation Threshold Optimization. We optimize only the translation threshold per trajectory to minimize: 1) overlaps between translation and gripper movements, and 2) spurious stop labels. We grid search over $\tau_{\text{trans}} \in [\tau_{\text{trans}}^{\text{init}} - 0.01, \tau_{\text{trans}}^{\text{init}} + 0.01]$ with 50 steps, minimizing:

$$\text{score} = 1.0 \times N_{\text{overlaps}} + 2.5 \times N_{\text{stops}}. \quad (6)$$

B.2. Gripper State Detection

Trajectory Segmentation. We segment the trajectory into chunks by detecting transitions in gripper state γ_t . Each chunk is labeled with its dominant gripper value: close (-1), open ($+1$), or idle (0).

Multi-Threshold Voting. To robustly detect gripper state changes, we run primitive extraction with three gripper thresholds: $[0.028, 0.03, 0.032]$. We extract the gripper dimension from each, average across thresholds, and round to obtain the final label $\in \{-1, 0, +1\}$ (close, idle, open). Note that this voting scheme is applied only to gripper state detection, not to movement primitives.

Filtering Abnormal States. We apply a post-filter to remove isolated idle segments that are surrounded by longer sequences

TABLE VII: Human evaluation of subtask decomposition quality on LIBERO.

Metric	Spatial	Object	Goal	Long	Average
Absolute Error (steps) ↓	4.2	3.5	8.0	7.2	5.7
Relative Error (%) ↓	3.9	2.5	5.8	3.0	3.8

of consistent gripper actions. Specifically, for an idle segment of length L , if $L_{\text{left}} + L_{\text{right}} > L$ where L_{left} and L_{right} are the lengths of consecutive consistent gripper actions (-1 or $+1$) on either side, we replace the idle segment with the surrounding value.

B.3. Movement Primitive Downsampling for LLM-based Subtask Boundary Inference

For trajectories whose length exceeds a fixed maximum threshold of 100 steps, we temporally downsample the movement primitive sequence before querying the LLM for subtask boundary inference. Specifically, given a trajectory of length $T > 100$, we uniformly sample indices with stride $\lceil T/100 \rceil$ to preserve global temporal structure. The LLM predicts subtask boundaries over the downsampled index set, which are then projected back to the original trajectory by linear index mapping.

B.4. Qualitative Results of Subtask-Decomposed Dataset

We show qualitative examples of our constructed subtask-decomposed dataset with timestamp boundaries (one example from each LIBERO task suite) in Fig. 5.

B.5. Human Evaluation

We evaluate the quality of the subtask-decomposed dataset via human annotation. For each LIBERO task suite, we randomly sample one demonstration from each of the 10 tasks (10 per suite, 40 total across four suites). For each sampled demonstration, human annotators inspect the subtask temporal boundaries predicted by the LLM and manually adjust the start and end timestamps when necessary.

We recruit five human evaluators. We report the mean absolute timestamp deviation between LLM-predicted and human-corrected boundaries and the relative boundary error, defined as the absolute timestamp deviation divided by the average subtask duration (i.e., trajectory length) for each subtask. Results in Table. VII demonstrate the precision of our pipeline; tasks with less distinct gripper state boundaries and high degrees of rotation (e.g., LIBERO-Goal) are more challenging to decompose into subtask trajectories.

C. IMPLEMENTATION DETAILS OF MBR DECODING

We sample $N=8$ hypotheses by re-running stochastic decoding with different random seeds, which changes the noise sampling in the diffusion action expert.

We compute the $N \times N$ pairwise L_2 distance matrix over trajectory features. Rather than selecting the hypothesis with

TABLE VIII: Finetuning hyperparameters for LIBERO.

Hyperparameter	Value
# GPUs	4 × NVIDIA A100 (40GB VRAM)
learning rate (LR)	5e-4 (decay to 5e-5 after 335K steps)
effective batch size	64 (2 per GPU, gradient accumulation of 8)
# train steps	500K
# diffusion steps	50
input images	1 third-person camera image, 1 wrist-mounted camera image
input image size	224 × 224 px
use observation history	no (use single-step inputs)
LoRA rank	32
action chunk size (H)	8 steps (predict 8, execute all 8 open-loop at test time)
action dimensions	9 (7 robot + 1 stop + 1 progress)
use proprio (robot state)	yes
use FiLM	no
# trainable parameters	313M total (111M LoRA adapter + 185M action head + 17M proprio projector)
last-action oversampling	8×
image augmentations	90% random crops, color jitter: <code>random_resized_crop=dict(scale=[0.9, 0.9], ratio=[1.0, 1.0]),</code> <code>random_brightness=[0.2], random_contrast=[0.8, 1.2],</code> <code>random_saturation=[0.8, 1.2], random_hue=[0.05]</code>

minimum average distance (standard MBR), we use a density-based variant that identifies the densest region and selects its medoid.

Adaptive r -NN Density Estimation. For each hypothesis, we compute its r -NN radius, the distance to its r -th nearest neighbor, as a local density estimate (smaller radius indicates higher density). We set r adaptively as:

$$r = \max\left(2, \min\left(4, \lfloor \sqrt{N} \rfloor\right)\right), \quad (7)$$

which yields $r=2$ for $N=8$.

Medoid Selection. We identify the densest point (smallest r -NN radius) as the pocket center, then find the medoid within this pocket—the hypothesis that minimizes average distance to other pocket members. This medoid is selected as the final action chunk for execution.

D. ADDITIONAL EXPERIMENTS AND DETAILS

Robust Stop and Progress Signal Detection. Since predicted stop (s_t) and progress (p_t) signals can be noisy, we apply a confirmation mechanism CONFIRM(\cdot) before triggering subtask transitions or VLM checks. A high signal refers to either $p_t \geq \tau_p$ (for progress) or $s_t = 1$ (for stop).

We track three quantities: 1) if a high signal has been observed (`first_seen`), 2) the count of consecutive high signals (c_{consec}), and 3) the number of low-signal steps since the last high signal (c_{gap}). A condition is confirmed if either:

$$c_{\text{consec}} \geq 2 \quad \text{or} \quad (\text{first_seen} \wedge c_{\text{gap}} \geq 2), \quad (8)$$

that is, two consecutive high signals, or a high signal that recurs after at least two low-signal steps. This filters isolated spurious predictions while remaining responsive to genuine transitions.

Training Hyperparameters. Hyperparameters for finetuning on VLA backbone of OpenVLA [66] with a diffusion-based action expert on LIBERO are listed in Table. VIII. For faster convergence, we decay the learning rate from 5e-4 to 5e-5 after 335K gradient steps.

Inference Hyperparameters. The VLM-based failure predictor is queried when subtask progress reaches $\tau_p = 0.9$. Each subtask allows up to $R = 3$ retries before forcing completion. We sample $N = 8$ hypotheses for MBR decoding with L_2 distance.

More Qualitative Results. We show more qualitative examples in Fig. 6.

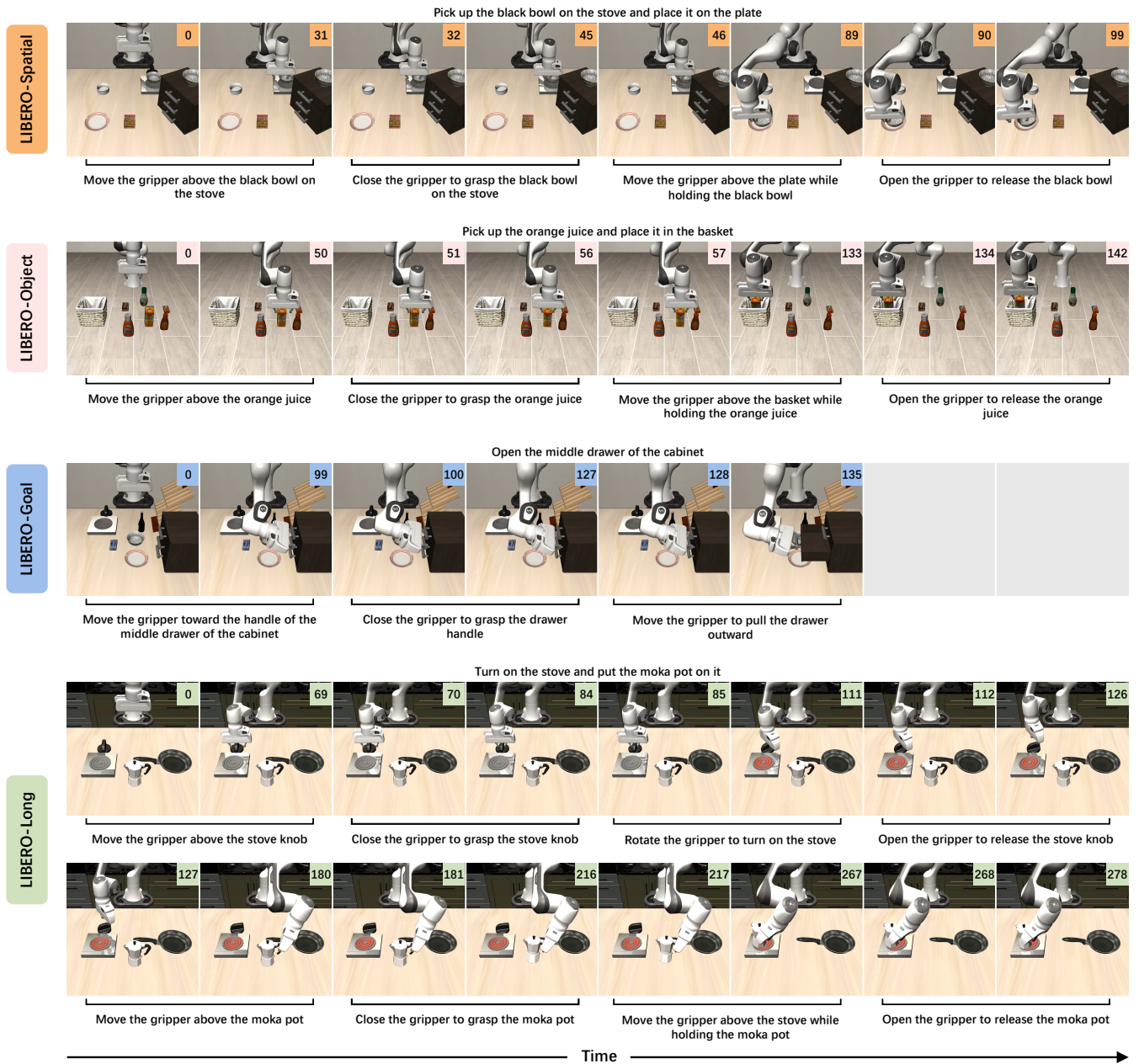


Fig. 5: Qualitative examples of subtask-decomposed dataset.

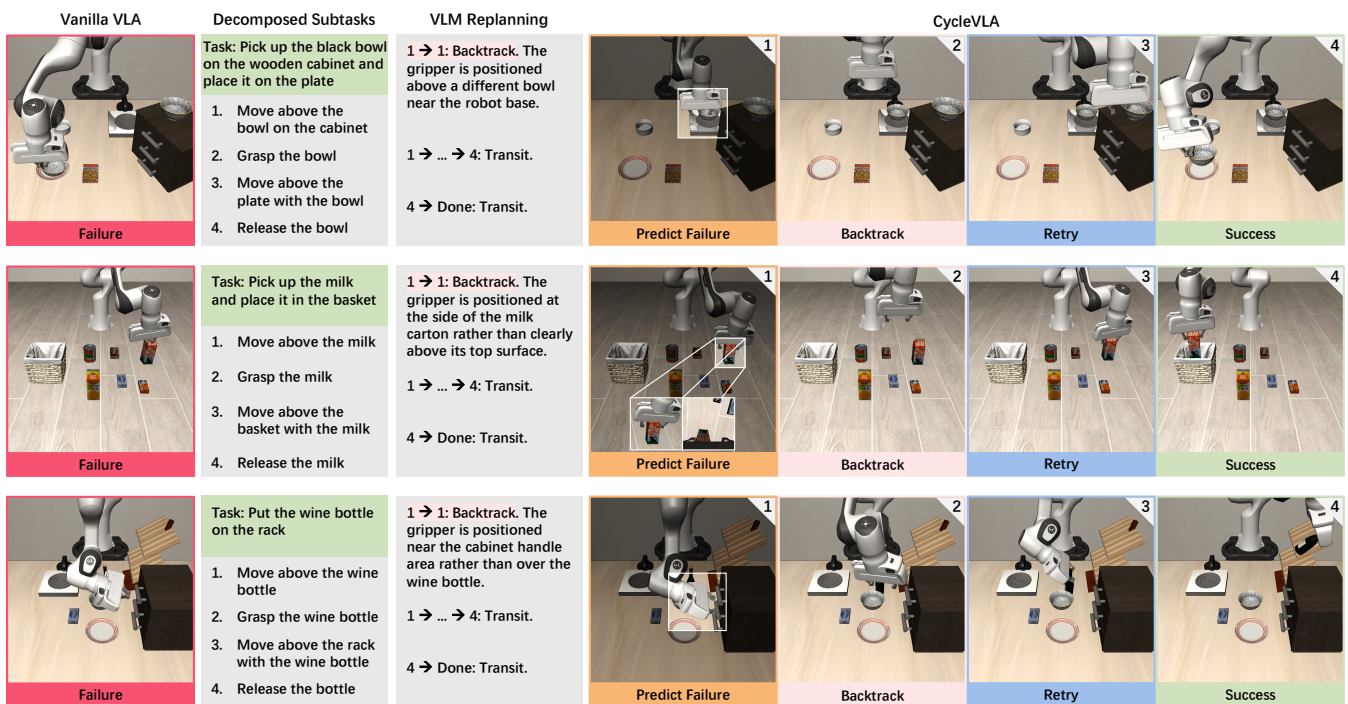


Fig. 6: Additional examples of CycleVLA.

E. PROMPT DETAILS OF SUBTASK DECOMPOSITION

We show exact prompts for LLMs to propose subtasks and infer their timestamp boundaries based on movement primitive sequence.

Subtask Proposal Prompt.

Input:

1. Task: {language_instruction}

Instruction:

You are given a high-level robotic task description. Your job is to decompose this task into a minimal set of formal subtasks that a robot must perform to complete the task.

Rules:

1. Minimal Subtask Decomposition

- Focus on the necessary and sufficient actions to complete the task.
- Do not over-decompose — prefer atomic but essential steps.
- Ask: What does the robot must do to succeed, regardless of variations in execution?

2. Object-Centric Reasoning

- Use the presence and spatial arrangement of objects as key indicators.
- Mention relative spatial cues (e.g., above the drawer handle) if implied in the task.

3. Skillset Usage and Formal Language

- Each subtask must begin with one of these actions (verbs):
 - 1) "Move the gripper ..."
 - 2) "Rotate the gripper ..."
 - 3) "Open the gripper ..."
 - 4) "Close the gripper ..."
- Keep language precise, formal, and robotic.
- As a rule of thumb:
 - 1) Move/Rotate is often followed by Close to grasp.
 - 2) Grasped objects are then moved, followed by Open to release.

Output Format:

Subtasks: ["<subtask_1>", "<subtask_2>", ...]

Reasoning: "<Explain how and why you chose each subtask based on the instruction>"

Subtask Timestamp Boundary Inference Prompt.

You are an expert reinforcement learning researcher. You have trained an optimal policy to control a robotic arm, which successfully completed a task as specified in natural language. The robot executed a sequence of actions to complete this task. Each action is recorded as a step in a trajectory.

Input:

1. Task: {language_instruction}

2. Subtasks list: {subtasks}

3. Trajectory features: Each entry in the dictionary corresponds to a single step on the trajectory and describes the move that is about to be executed.

trajectory_features = {0: "<move_primitive>", 1: "<move_primitive>", ...}

Instruction:

Decompose the entire trajectory into subtasks and assign a start and end step index to each subtask. The goal is to produce a mapping of the form:

Labeled_dict = {"subtask_1": [start_idx, end_idx], "subtask_2": [start_idx, end_idx], ...}

Rules:

1. Noisy Labels

- The trajectory data contains noise. Apply the following rules carefully:
- "stop" labels often appear even when the robot is still moving.

- Treat "stop" as movement if it appears between meaningful motion steps.
 - Do NOT segment a new subtask just because you see a "stop".
 - "open/close gripper" labels that persist for very short durations may be noise. However, gripper actions are generally more reliable than motion primitives.
2. Robust Labeling Strategies
 - Brief, short, inconsistent movement descriptions that conflict with prior and subsequent steps are likely to be noise.
 - Cross-reference other movement labels to decide whether a short-duration label is meaningful or just noise.
 3. Exhaustive Coverage
 - You must not skip any steps. Every step in the trajectory should be assigned to exactly one subtask.
 - There should be no gaps in the index ranges. Subtasks must be labeled sequentially and cover the entire range of the trajectory indices.

Output Format:

Labeled_dict: {"subtask_1": [start_idx, end_idx], "subtask_2": [start_idx, end_idx], ...}

Reasoning: "<Explain your logic for identifying and segmenting each subtask>"

F. PROMPT DETAILS OF FAILURE PREDICTOR AND PLANNER

We show exact prompts for VLMs to predict failure and plan recovery at subtask boundaries.

VLM Failure Prediction and Planning Prompt.

You are an expert robot behavior annotator. Decide what the robot should do next given it is ~90% through the current subtask. Your job is to FORECAST whether the current subtask will likely succeed if we continue without corrective repositioning.

Input:

1. Task instruction: {language_instruction}
2. Subtask list: {subtasks}
3. Current subtask: {current_subtask}
4. Visual inputs (two synchronized views):
 - FRONT: third-person view (global alignment, object identity, spatial relations)
 - WRIST: close-up gripper view (detailed contact, local geometry, physical affordances)

Decision Rule (forecasting at ~90%):

- Default to transit when success appears reasonably likely within the next few actions without corrective repositioning.
- Choose backtrack if strong, unambiguous visual evidence indicates that the subtask will fail without repositioning.

View-Specific Fusion Instruction:

- FRONT view provides global context: object identity, pose, global alignment, reachability, and path clearance.
- WRIST view provides local interaction cues: gripper orientation, contact points, slip, stability, and detailed positioning relative to affordances.
- Combine both views to reason about functional success: whether the current configuration supports the intended physical interaction (e.g., grasping, pulling, pushing).
- FRONT dominates for global spatial reasoning and goal reachability.
- WRIST dominates for local contact accuracy and grasp quality.

Affordance Reasoning Guidance:

- Evaluate whether the gripper's pose is consistent with the object's intended use:
 - 1) For a bowl: grasping the edge or rim is acceptable and often intended for lifting.
 - 2) For a drawer: alignment with the handle is the key indicator of readiness.
 - 3) For a push or pull action: confirm direction and surface contact match the required motion.
- Do not penalize partial or asymmetric contacts if they serve a valid affordance and appear stable.

Wrong Object or Wrong Subtask Detection:

- In addition to misalignment, detect late-stage "silent failures" involving wrong object engagement or wrong subtask execution.

- If visual evidence indicates the gripper is interacting with an unintended object, target, or affordance (e.g., lifting or contacting a distractor, manipulating the wrong receptacle, or committing to a different subtask's goal), output type: backtrack.
- Set next_subtask to the earliest subtask that restores correct target selection and preconditions (typically a reach, align, or target-identification step, NOT a trivial open/close gripper).

Backtracking Target:

- Backtrack to the earliest subtask that restores the missing precondition (typically a positioning or alignment step that enables correct affordance engagement).

Output Format:

next_subtask: <exact subtask from subtasks list>

type: <transit / backtrack>

reason: <explain in a concise paragraph, justifying the decision>

front_view_evidence:

- <concise observable cue 1>
- <concise observable cue 2>
- <concise observable cue 3>
- <concise observable cue 4>

wrist_view_evidence:

- <concise observable cue 1>
- <concise observable cue 2>
- <concise observable cue 3>
- <concise observable cue 4>

assessment:

- success_likelihood: <high | medium | low>
- key_risks: <comma-separated brief phrases>
- view_agreement: <agree | partial | disagree>; <short phrase on which view dominates and why>
- decision_basis: <short phrase linking likelihood + dominant cues to decision>

Constraints:

- Focus strictly on observable visual and physical evidence.
- Keep each bullet concise (≤ 12 words).
- Use exact strings from subtasks for next_subtask.
- type must be either transit or backtrack.
- Return only the specified fields; no extra commentary.